Artifacts in 3-Tesla MRI: Physical background and reduction strategies

Olaf Dietrich, PhD[1], Maximilian F. Reiser, MD[1], and Stefan O. Schoenberg, MD[2]

[1] Department of Clinical Radiology – Grosshadern, Ludwig Maximilian University of Munich, Germany

[2] Institute of Clinical Radiology and Nuclear Medicine, University Hospital Mannheim, Medical Faculty Mannheim – University of Heidelberg, Mannheim, Germany

Final version: *Eur J Radiol* 2008; **65**(1): 29–35. <URL:http://dx.doi.org/10.1016/j.ejrad.2007.11.005>

Abstract

Magnetic resonance imaging (MRI) at a field strength of 3 Tesla has become more and more frequently used in recent years. In an increasing number of radiological sites, 3-Tesla MRI now starts to play the same role for clinical imaging that was occupied by 1.5-Tesla systems in the past. Because of physical limitations related to the higher field strength and because of protocols transferred from 1.5-Tesla MRI that are not yet fully optimized for 3 Tesla, radiologists and technicians working at these systems are relatively often confronted with image artifacts related to 3-Tesla MRI. The purpose of this review article is to present the most relevant artifacts that arise in 3-Tesla MRI, to provide some physical background on the formation of artifacts, and to suggest strategies to reduce or avoid these artifacts. The discussed artifacts are classified and ordered according to the physical mechanism or property of the MRI system responsible for their occurrence: artifacts caused by B0 inhomogeneity and susceptibility effects, B1 inhomogeneity and wavelength effects, chemical-shift effects, blood flow and magnetohydrodynamics, and artifacts related to SNR.

Keywords:

Magnetic resonance imaging; 3-Tesla MRI; High-field MRI; Image artifacts

Corresponding author:

Olaf Dietrich, PhD
Radiological Physics
Department of Clinical Radiology – Grosshadern
Ludwig Maximilian University of Munich
Marchioninistr. 15, 81377 Munich, GERMANY
Phone: +49-89-7095-3623
Fax: +49-89-7095-4627
E-mail: od@dtrx.net

Introduction

Magnetic resonance imaging (MRI) systems working at a field strength, B_0, of 3 Tesla have become more and more frequent in recent years. In an increasing number of radiological sites, 3-Tesla MRI starts to play the same role for clinical imaging that was occupied by 1.5-Tesla systems for about the last 10 years[1–10]. The main motivation for the transition from 1.5-Tesla to 3-Tesla MRI systems is the improved signal-to-noise ratio (SNR), which is approximately proportional to the field strength[11], B_0; thus, under ideal conditions and with optimized acquisition techniques a doubled SNR can be expected at 3 Tesla in comparison to 1.5 Tesla. The growing availability of 3-Tesla MRI systems is for instance demonstrated by the number of publications on 3-Tesla MRI listed in the Medline database, which increased from around 30 in the year 2000 to more than 400 in 2006.

In the 1990s, 3-Tesla MRI was available predominantly in a small number of specialized neuroradiological or neuropsychiatric research sites. Typical applications included functional MRI[12] or spectroscopy studies of the brain, which were performed with optimized protocols and under attendance of specialized engineers or physicists. Today, the availability of 3-Tesla MRI systems has substantially broadened and these systems are applied for imaging of all anatomical areas including e.g. musculoskeletal[7, 8], abdominal[4, 9], cardiac[5], angiographic[1, 2], and whole-body imaging[3, 6]. This development leads to an increasing diversity of applied pulse sequences and protocols, which are not always fully optimized for 3-Tesla MRI. Consequently, the radiologist or technician working with such 3-Tesla protocols will comparatively frequently be confronted with image artifacts related to 3-Tesla MRI[13, 14].

The purpose of this review article is to present the most relevant artifacts that arise in 3-Tesla MRI, to provide some physical background on the formation of artifacts, and to suggest strategies to reduce or avoid these artifacts. The discussed artifacts are classified and ordered according to the physical mechanism or property of the MRI system responsible for their occurrence: In the following sections, we distinguish artifacts caused by B_0 inhomogeneity and susceptibility effects, B_1 inhomogeneity and wavelength effects, chemical-shift effects, blood flow and magnetohydrodynamics, and artifacts related to SNR.

Artifacts

B_0 inhomogeneity and susceptibility effects

An extremely homogeneous static magnetic field, B_0, is required around the isocenter of the magnet for magnetic resonance imaging. The homogeneity of the static magnetic field influences the distribution of the Larmor frequencies of the protons and also the linearity of the magnetic field gradients required for spatial encoding. If the static magnetic field is disturbed, different effects of reduced B_0 homogeneity can be observed: Variations of the Larmor frequency within a single voxel result in dephasing of the spins and, thus, in signal loss in acquired gradient echoes. This effect is quantified by the relaxation time, T_2^*, which becomes shorter with increasing microscopic field inhomogeneity[15, 16]. Medium-scale or large-scale variations of the Larmor frequency result in geometric distortion artifacts or mismatch of the excitation frequency of chemically selective radio-frequency (RF) pulses and the resonance frequency of the protons. The latter may lead, e.g., to incomplete fat saturation after the application of frequency-selective fat-saturation pulses.

Generally, the B_0 homogeneity of the (empty) magnet itself is very high; a typical value specified by the magnet manufacturers is a homogeneity of 1 ppm (i.e. 0.001 ‰) in a 50-cm-diameter spherical volume around the isocenter. Unfortunately, the originally very high homogeneity of the magnetic field is substantially reduced by the patient (or any phantom) inside the magnet because of a physical property called susceptibility. The magnetic susceptibility describes the extent to which a material placed in an external magnetic field becomes magnetized itself. The susceptibility varies substantially for different materials such as air, water, or different biological tissues. As a consequence, the additional magnetic fields of the materials inside the magnet are superposed to the originally homogeneous B_0 field resulting in decreased overall field homogeneity. While large-scale variations of the field can be partly compensated by the shimming of the field, all other inhomogeneities are inevitable and result in artifacts depending on the pulse sequence and acquisition parameters.

Unfortunately, the effects of susceptibility variations are proportional to the field strength, B_0; i.e., twice as large frequency variations are found at 3 Tesla than at 1.5 Tesla[13, 14, 17, 18]. Therefore, all kind of susceptibility artifacts appear much more pronounced in 3-Tesla MRI than at lower field strengths[19]. An important manifestation of a susceptibility-related artifact is the signal loss in gradient-echo images around metallic implants or surgical clips such as clips from prior cholecystectomy[20]. To reduce these artifacts, the echo time, TE, of the pulse sequence should be decreased[21] and the receiver bandwidth increased. Although these artifacts are more pronounced at 3 Tesla and may obscure visualization of important anatomic structures, such as the biliary ductal system, Merkle et al. conclude that biliary pseudo-obstructions due to susceptibility artifacts from cholecystectomy surgical clips are not substantially more common on 3-T MR cholangiography in clinical practice than at 1.5 Tesla[20].

Another consequence of susceptibility variations are geometric distortions in echo-planar imaging (EPI) at interfaces between soft tissue and bone or air as, e.g., in the base of the skull or in the head-and-neck region (Fig. 1). These distortions can be reduced by decreasing the echo spacing of the readout train (e.g. by increasing the receiver bandwidth) or by applying parallel-imaging techniques to reduce the echo-train length (Fig. 1c).

As mentioned above, the efficacy of frequency-selective fat-saturation pulses can also be decreased due to B_0 inhomogeneities as demonstrated in Fig. 2. In some cases, these artifacts can be mitigated by improved field shimming e.g. by repeating the automatic shim with a more specific shim volume. Generally, these effects are more pronounced the further the image slice is positioned from the isocenter of the magnet; thus, optimal positioning of the patient in z-direction is recommendable to reduce these artifacts.

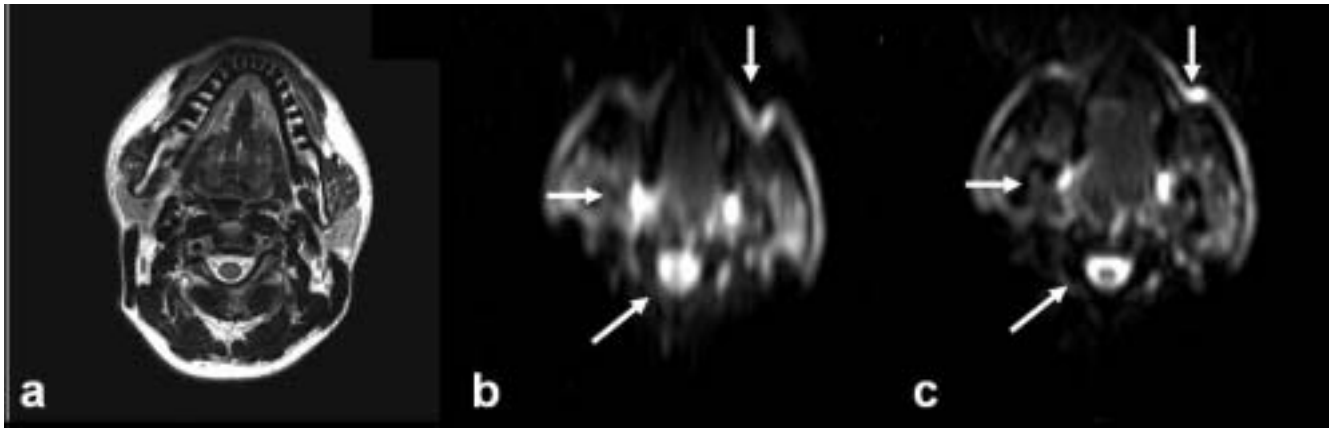

Figure 1: Geometric distortions of 3-Tesla EPI acquisitions in the head-and-neck region at interfaces between soft tissue and bone or air. (a) Reference fast-spin-echo acquisition without distortions; (b) EPI acquisition of the same slice without parallel imaging, severe distortion artifacts are visible (arrows); (c) EPI acquisition with acceleration factor 2, distortion artifacts are still present but considerably reduced (arrows).

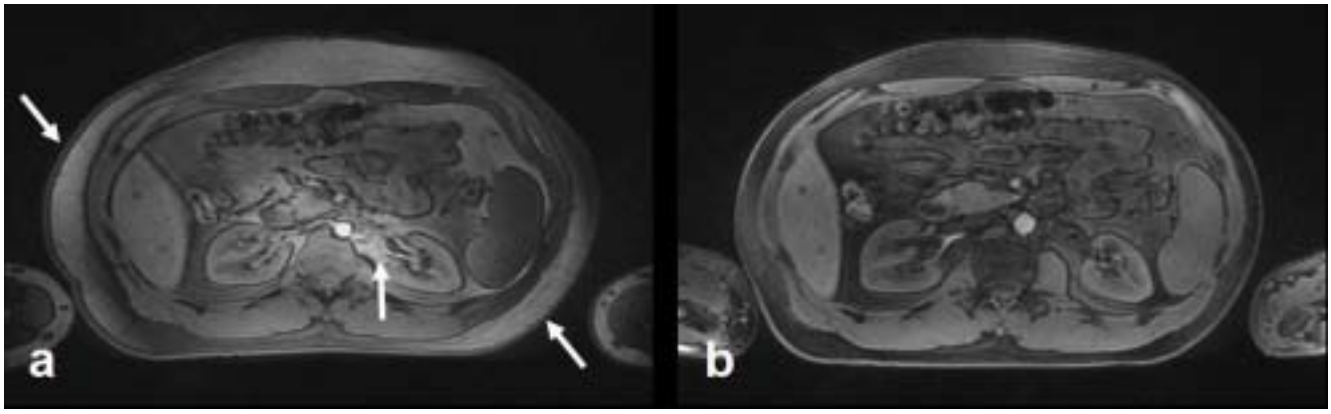

Figure 2: Reduced efficacy of frequency-selective fat-saturation pulses due to B_0 inhomogeneities at 3 Tesla. (a) Acquisition at off-center position with insufficient fat suppression (arrows), (b) identical acquisition at isocenter.

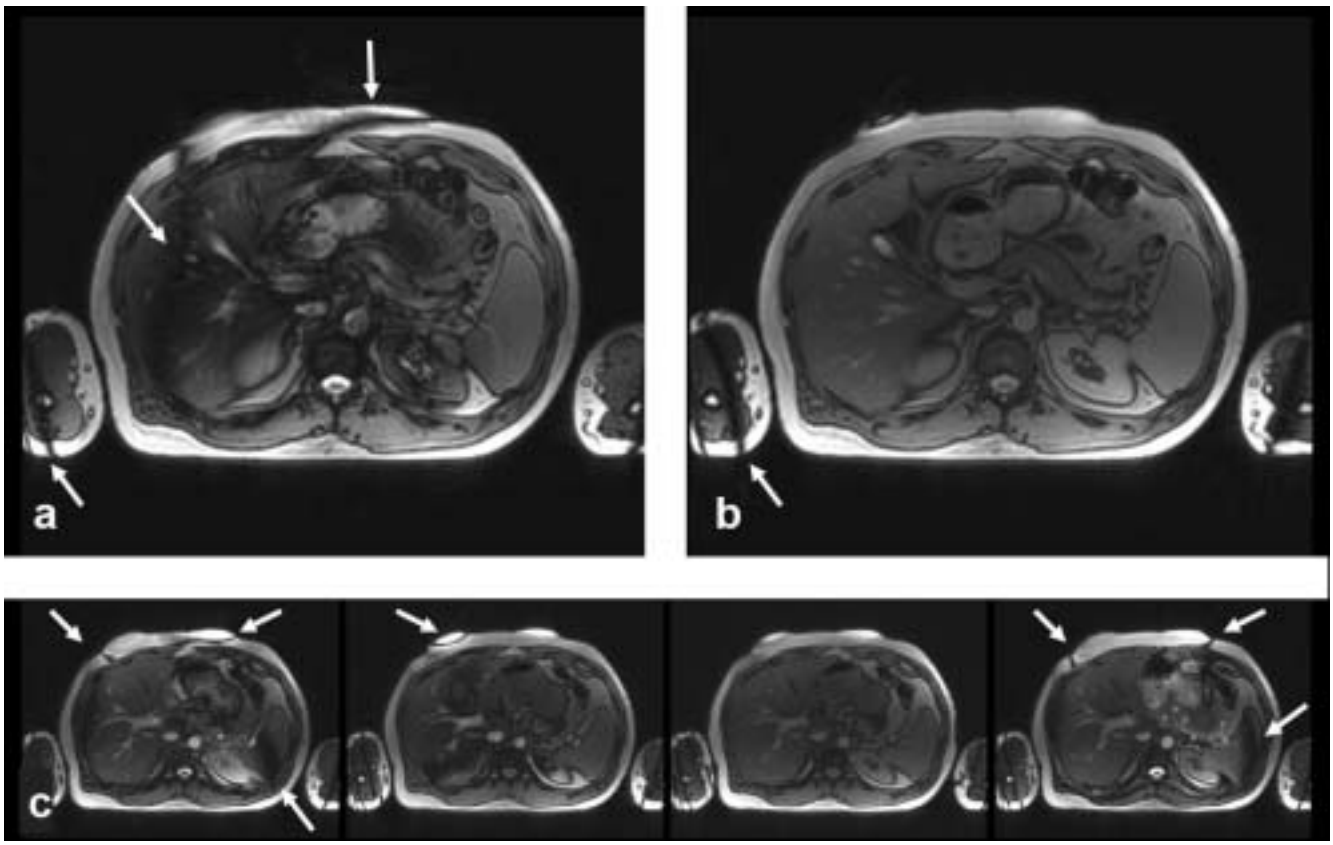

Figure 3: Band-shaped signal losses (arrows) in steady-state free-precession (SSFP) sequences due to B_0 inhomogeneities. (a) Banding artifacts compromising liver imaging. (b) Acquisition with identical parameters but with optimized frequency offset to shift artifacts out of region of interest. (c) Series of frequency-scout images demonstrating frequency-depending artifact positions.

Steady-state free-precession (SSFP) sequences are also very sensitive to B_0 inhomogeneities as shown in Fig. 3a. Relatively small frequency shifts lead to substantial reduction of the transversal steady-state magnetization and, thus, to band-shaped signal losses in the image[22]. In many cases, these off-resonance or banding artifacts cannot be fully avoided, but it may be possible to move the artifacts out of the current region of interest, e.g. in cardiac or abdominal MRI[23–25] (Fig. 3b). This is done by applying a frequency offset to the nominal resonance frequency; the optimal offset frequency can be determined by a so-called frequency scout, i.e. a series of SSFP images acquired with several different offset frequencies (Fig. 3c).

B_1 inhomogeneity and wavelength effects

The term "(electromagnetic) B_1 field" is frequently used to refer to the radio-frequency fields involved in MR imaging and in particular to the field of the transmitted RF excitation pulses. Spatial inhomogeneity of the B_1 field results in flip-angle deviations depending on the spatial position, i.e. instead of a nominal 90° excitation pulse of a spin-echo sequence or a 10° flip angle of a gradient-echo sequence, the actual flip angle can be substantially lower in certain areas of the acquired volume. This often leads to reduced signal intensity in these areas or to altered contrast particularly in FLASH sequences whose T_1-weighting depends on the flip angle[26]. Further effects of B_1 inhomogeneity are locally insufficient magnetization preparation with inversion and saturation pulses if the actual flip angles deviate from 180° and 90°, respectively[27]. The same mechanism can also influence frequency-selective fat saturation resulting in insufficient suppression of the fat signal similarly as described above in the presence of B_0 inhomogeneities.

The B_1 homogeneity depends on the design of the transmit coils as well as on the relation of the imaged object and the RF wavelength. While well-designed transmit coils should provide sufficiently homogeneous B_1 fields in both 1.5-Tesla and 3-Tesla MRI, the influence of the wavelength becomes much more relevant at 3 Tesla[28]. The wavelength of the RF field in air is about 468 cm and 234 cm at 1.5 T and 3 T, respectively[13, 14]. However, the wavelength in tissue is substantially reduced because of the much higher dielec-

tric constant of tissue compared to air. The dielectric constant in biological tissue ranges between 10 and 100, resulting in wavelengths reduced by a factor calculated as the inverse of the dielectric constant, i.e., of 0.1 to 0.01. If the wavelength of the RF field is in the same order of magnitude as the geometric dimensions of the imaged object then constructive or destructive interferences of the transmitted RF field may be observed resulting in either regional (e.g. central) brightening or regional signal loss, respectively. These effects appear much more frequently at 3 Tesla than at 1.5 Tesla because the RF wavelength at 3 Tesla is only half as large as at 1.5 Tesla and, thus, is more frequently of the same size as the imaged anatomic structures. In the past, these effects have sometimes been called “dielectric resonance effects”, but recent publications favor the terms “standing-wave effects” or “RF interferences”[29].

The signal loss due to wavelength effects at 3-Tesla MRI is demonstrated in Fig. 4a; as in this example, relatively slim or athletic patients are more often affected by this artifact than more obese patients. Often these effects can be mitigated by an additional dielectric pad or cushion positioned on the abdomen of the patient (Fig. 4b). These simple devices modify the geometry of the imaged volume and thus can reduce RF interference effects. It can also be helpful to manually modify the RF-transmitter amplitude in order to reduce B_1-inhomogeneity -induced signal loss. The automatic calibration of the RF-transmitter amplitude may be biased by B_1 inhomogeneity effects and an improved flip-angle distribution can sometimes be obtained by manually increasing the transmitter amplitude. In combination with post-processing filters that provide a more uniform signal distribution, image quality can be considerably improved (Fig. 5).

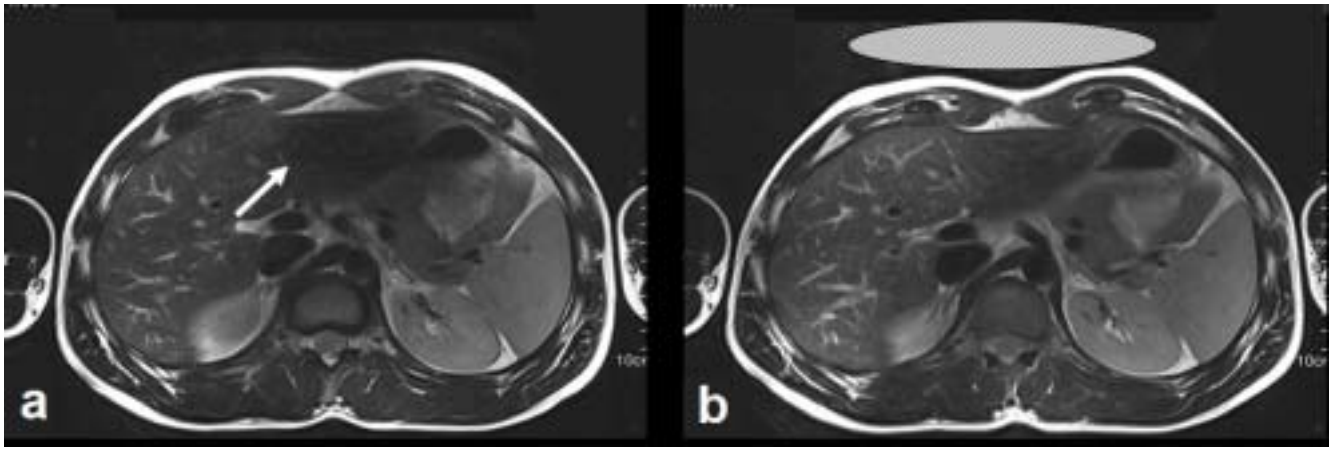

Figure 4: Signal loss due to wavelength effects at 3 Tesla. (a) Destructive RF interference results in reduced signal intensity in the abdomen (arrow), particularly in slim or athletic patients. (b) This effect can be mitigated by positioning a dielectric cushion on the abdomen of the patient. Images courtesy of W. Horger, Siemens Medical Solutions, Germany.

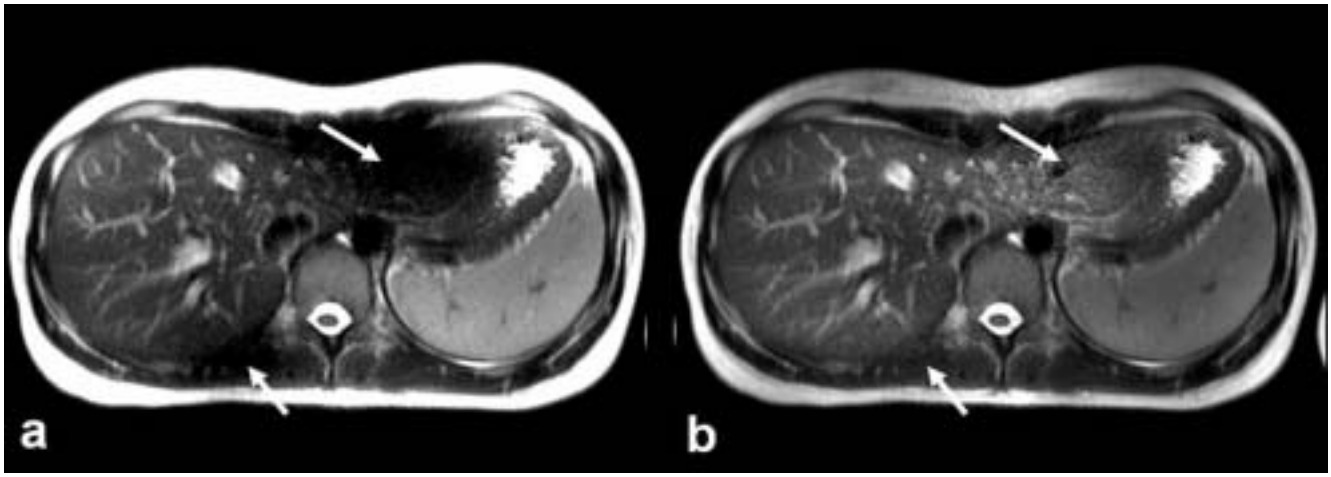

Figure 5: Signal loss due to inhomogeneous flip-angle distribution at 3 Tesla. (a) Wavelength effects result in reduced signal intensity in the abdomen (arrows). (b) This effect can in some cases be reduced by manually increasing the RF-transmitter amplitude (here by 50 %) and by applying image post-processing filters to obtain more uniform image intensities. Images courtesy of W. Horger, Siemens Medical Solutions, Germany.

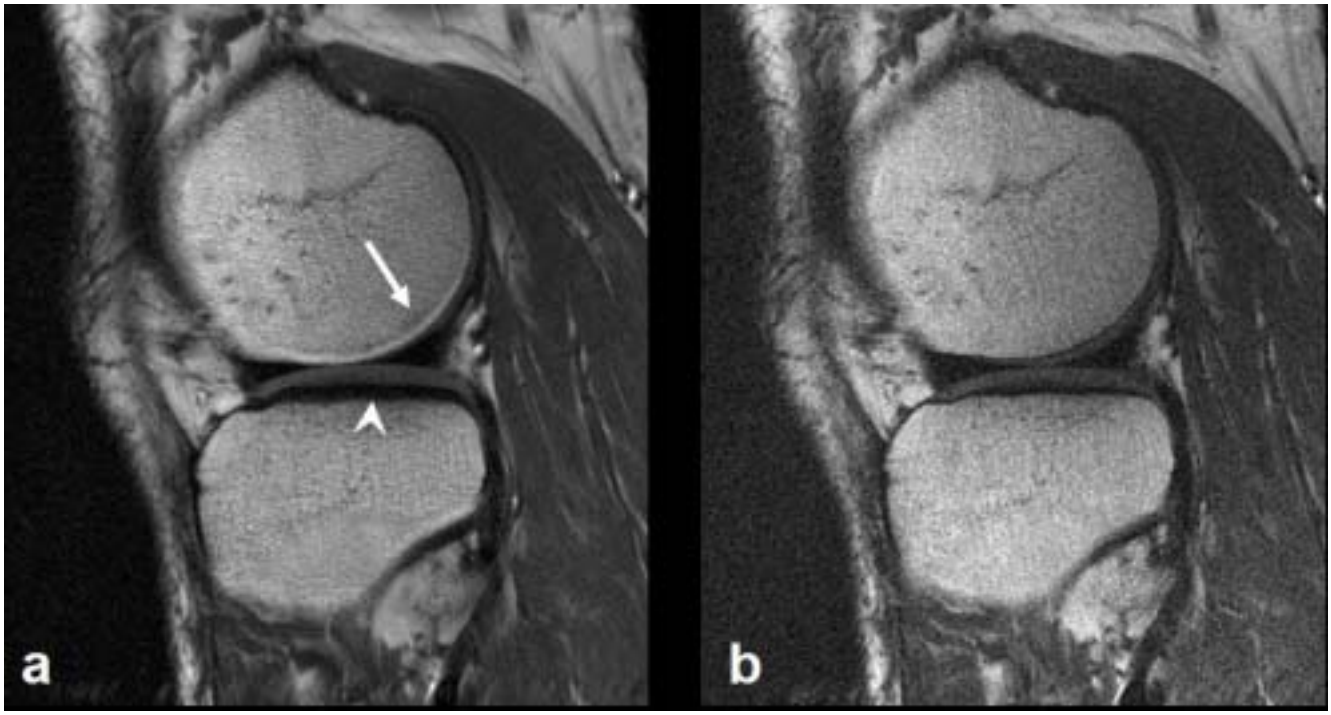

Figure 6: (a) Chemical-shift artifact of the first kind resulting in a geometrical shift of fat-containing bone marrow relative to cartilage (arrow head) and the image-compromising superposition of bone marrow onto cartilage (arrow); receiver bandwidth: 70 Hz/pixel. (b) Identical acquisition with increased receiver bandwidth of 350 Hz/pixel in order to reduce the chemical-shift artifact at the cost of a reduced SNR.

More advanced techniques for B_1-field homogenization are currently under development. If RF pulses are appropriately modulated in amplitude and phase during the application of time-varying gradients, RF excitation can be spatially tailored in order to compensate for B_1 inhomogeneity[30]. Currently the combination of this approach with RF transmit-coil arrays and parallel-excitation techniques is investigated[31–33].

Chemical-shift effects

Protons in different molecules have specific characteristic Larmor frequencies; this property is called "chemical shift" and is exploited in magnetic resonance spectroscopy in order to differentiate the molecules in a sample. For magnetic resonance imaging in vivo, there are essentially only two important groups of molecules with differing Larmor frequencies: protons in water and protons in fat tissue. The difference of the Larmor frequencies of these protons is approximately 3.5 ppm. Since the spatial position in MRI is encoded using varying Larmor frequencies induced by the applied magnetic gradient pulses, the chemical shift leads to a slight geometric shift of the relative position of water and fat protons in readout direction. This effect is called chemical-shift artifact of the first kind[14]. The extent of this shift depends on the receiver bandwidth and is, for a fixed receiver bandwidth, proportional to the field strength[34], B_0. Thus, the observed chemical shift at 3 Tesla is twice as large as at 1.5 Tesla and can result in the image-compromising superposition of fat tissue onto other tissues next to it as demonstrated in Fig. 6a.

There are several possibilities to avoid or reduce signal superposition due to the chemical-shift effect. Depending on the anatomical situation it may be possible either to switch readout and phase-encoding direction or to inverse the polarity of the readout gradient in order to obtain a less compromising signal superposition. To reduce the chemical-shift artifact to the same level as in 1.5-Tesla MRI, the receiver bandwidth of the pulse sequence can be doubled[35]. This will decrease the SNR of the acquisition by about 30 % (to $1/\sqrt{2} = 70.7\%$ of the original SNR), but in comparison to 1.5 Tesla, there is still a remaining increase in SNR by about 40 %. The influence of the receiver bandwidth on the chemical-shift artifact is demonstrated in Fig. 6b.

The chemical-shift artifact of the second kind is observed as a hypointense rim, e.g. around organs embedded in fat tissue such as the kidneys when imaged in opposed-phase condition[14]. This artifact is the result

of signal cancellation of water and fat protons within the same voxel. It appears identical independent of the field strength, if the echo time in each case is chosen correctly for opposed-phase imaging. The different Larmor frequencies at 1.5 Tesla and 3 Tesla, however, result in different in-phase and opposed-phase conditions. This means that instead of opposed-phase echo times of 2.2, 6.7, 11.2 ms, … at 1.5 Tesla, TEs of 1.1, 3.4, 5.6 ms, … fulfill the opposed-phase condition at 3 Tesla.

Blood flow and magnetohydrodynamic effect

The flow of blood ions perpendicular to the strong static magnetic field, B_0, gives rise to induced voltages and currents; this mechanism is called the magnetohydrodynamic effect[36]. The voltages and currents are proportional to the field strength, B_0. Although the induced voltages are relatively small, they can influence the ECG signal required e.g. for cardiac gating[37]. Indeed is the quality of the ECG signal in 3-Tesla scanners generally worse than in 1.5-Tesla scanners[38], and improved algorithms are required to correctly identify the R wave.

An image artifact that is possibly related to the magnetohydrodynamic effect is the signal loss in the pulmonary vessels acquired with a single-shot fast-spin-echo sequence without ECG gating at 3 Tesla (Fig. 7a). These vessels are generally visible at 1.5 Tesla without ECG gating (Fig. 7b); however, at 3 Tesla, ECG gating to the diastolic phase is required to obtain similar images (Fig. 7c). Blood pulsation in the static magnetic field, B_0, induces electric currents and associated additional magnetic fields that may be the cause for dephasing of the spins in and around the pulmonary vessels.

SNR-related artifacts

Certain artifacts at 3 Tesla are observed as a consequence of the improved signal-to-noise ratio in comparison to 1.5-Tesla MRI. In these cases, the artifacts have relatively low intensity, i.e. the artifact-to-noise ratio (ANR)[13] is low, and the artifacts are masked by the statistical image noise at 1.5 Tesla. A typical example is the occurrence of Gibbs ringing artifacts (Fig. 8) at 3 Tesla that has not been visible at lower field strengths. Gibbs ringing is caused by data clipping at the edges of k-space, i.e. rawdata signal intensities that are still substantially over the noise level at the borders of the acquired k-space[39]. Obviously, this is more often the case at higher field strengths with proportionally increased signal-to-noise ratio. Gibbs ringing can be reduced by either increasing the spatial resolution or by applying reconstruction filters such as the Hanning filter to smoothly reduce the signal at the edges of k-space.

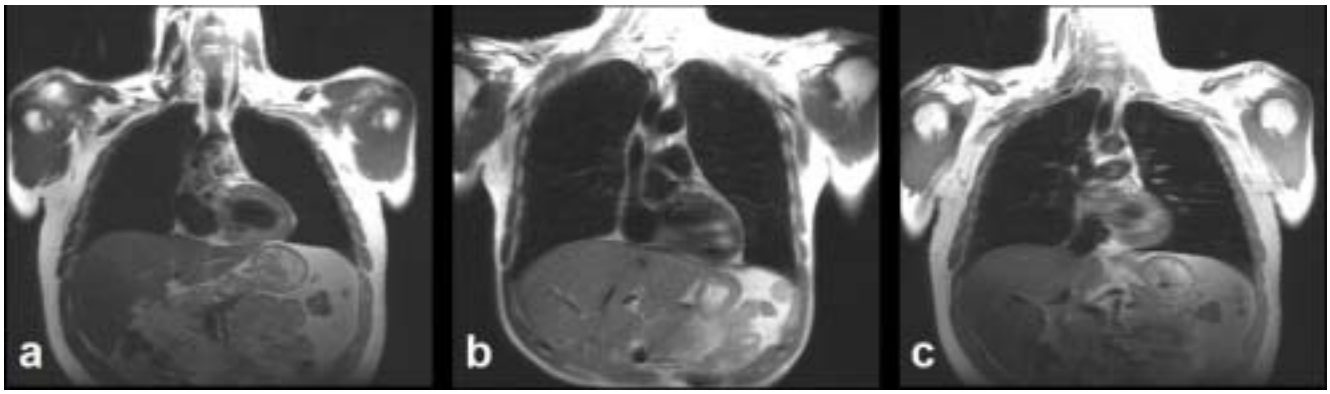

Figure 7: (a) Signal loss in the pulmonary vessels in non-gated 3-Tesla single-shot fast-spin-echo (FSE) acquisition possibly related to the magnetohydrodynamic effect. (b) Non-gated 1.5-Tesla single-shot FSE acquisition demonstrating visual signal in pulmonary vessels. (c) Gated 3-Tesla single-shot FSE acquisition of the same volunteer as in (a) with data acquisition during diastole; the vessel signal is restored.

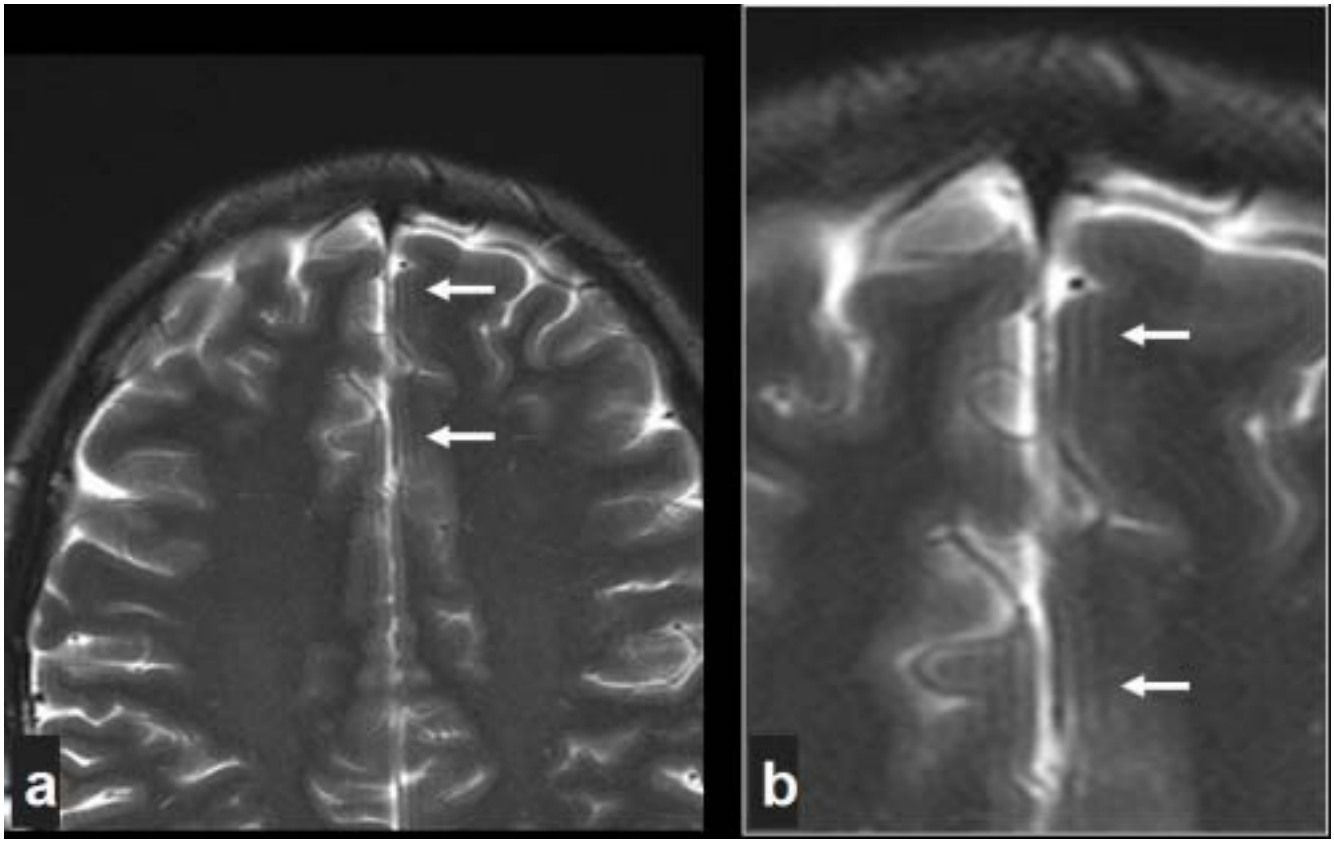

Figure 8: (a) Gibbs ringing artifacts in T2-weighted 3-Tesla FSE acquisition may be observed as a consequence of the improved signal-to-noise ratio in comparison to 1.5-Tesla MRI; (b) magnified detail view of (a).

Conclusions

Generally, a larger number of artifacts must still be expected in 3-Tesla MRI than in routine 1.5-Tesla imaging. These artifacts are caused either by physical limitations related to the higher field strength or by protocols transferred from 1.5-Tesla MRI that are not yet fully optimized for the higher field strength. Most artifacts, however, can be mitigated or avoided by small modifications of the pulse sequences such as adapted receiver bandwidths or echo times, by new techniques such as parallel imaging, by small additional devices such as dielectric cushions, or by improved techniques e.g. for ECG signal analysis or raw-data post-processing. By the combined effort of radiologists and MR physicists or engineers, an artifact level comparable to 1.5 Tesla can be accomplished while preserving most of the additional signal-to-noise ratio (or the corresponding gain in acquisition time) enabled by 3-Tesla MRI. Our own experience with whole-body 3-Tesla MR applications is that 3-Tesla MRI is now fully suitable for clinical routine imaging of virtually all anatomic regions providing an image quality that is at least comparable and frequently superior to 1.5-Tesla MRI.

References

[1] Kramer U, Nael K, Fenchel M, Miller S. Magnetic resonance angiography of chest and abdomen at 3 T. Top Magn Reson Imaging 2007;18(2):105-15.

[2] Kramer H, Michaely HJ, Reiser MF, Schoenberg SO. Peripheral magnetic resonance angiography at 3.0 T. Top Magn Reson Imaging 2007;18(2):135-8.

[3] Nael K, Fenchel MC, Kramer U, Finn JP, Gruehm S. Whole-body contrast-enhanced magnetic resonance angiography: new advances at 3.0 T. Top Magn Reson Imaging 2007;18(2):127-34.

[4] Michaely HJ, Kramer H, Attenberger U, Sourbron SP, Weckbach S, Reiser MF, Schoenberg SO. Renal magnetic resonance angiography at 3.0 T: technical feasibility and clinical perspectives. Top Magn Reson Imaging 2007;18(2):117-25.

[5] Fenchel M, Kramer U, Nael K, Miller S. Cardiac magnetic resonance imaging at 3.0 T. Top Magn Reson Imaging 2007;18(2):95-104.

[6] Schmidt GP, Kramer H, Reiser MF, Glaser C. Whole-body magnetic resonance imaging and positron emission tomography-computed tomography in oncology. Top Magn Reson Imaging 2007;18(3):193-202.

[7] Shapiro MD. MR imaging of the spine at 3T. Magn Reson Imaging Clin N Am 2006;14(1):97-108.

[8] Ramnath RR. 3T MR imaging of the musculoskeletal system (Part II): clinical applications. Magn Reson Imaging Clin N Am 2006;14(1):41-62.

[9] Merkle EM, Dale BM, Paulson EK. Abdominal MR imaging at 3T. Magn Reson Imaging Clin N Am 2006;14(1):17-26.

[10] Hussain SM, van den Bos IC, Oliveto JM, Martin DR. MR imaging of the female pelvis at 3T. Magn Reson Imaging Clin N Am 2006;14(4):537-44.

[11] Edelstein WA, Glover GH, Hardy CJ, Redington RW. The intrinsic signal-to-noise ratio in NMR imaging. Magn Reson Med 1986;3(4):604-18.

[12] Thulborn KR. Clinical rationale for very-high-field (3.0 Tesla) functional magnetic resonance imaging. Top Magn Reson Imaging 1999;10(1):37-50.

[13] Bernstein MA, Huston J 3rd, Ward HA. Imaging artifacts at 3.0T. J Magn Reson Imaging 2006;24(4):735-46.

[14] Merkle EM, Dale BM. Abdominal MRI at 3.0 T: the basics revisited. AJR Am J Roentgenol 2006;186(6):1524-32.

[15] Haacke EM, Tkach JA, Parrish TB. Reduction of T2* dephasing in gradient field-echo imaging. Radiology 1989;170(2):457-62.

[16] Yablonskiy DA, Haacke EM. Theory of NMR signal behavior in magnetically inhomogeneous tissues: the static dephasing regime. Magn Reson Med 1994;32(6):749-63.

[17] Schenck JF. The role of magnetic susceptibility in magnetic resonance imaging: MRI magnetic compatibility of the first and second kinds. Med Phys 1996;23(6):815-50.

[18] Lewin JS, Duerk JL, Jain VR, Petersilge CA, Chao CP, Haaga JR. Needle localization in MR-guided biopsy and aspiration: effects of field strength, sequence design, and magnetic field orientation. AJR Am J Roentgenol 1996;166(6):1337-45.

[19] Graf H, Lauer UA, Berger A, Schick F. RF artifacts caused by metallic implants or instruments which get more prominent at 3 T: an in vitro study. Magn Reson Imaging 2005 Apr;23(3):493-9.

[20] Merkle EM, Dale BM, Thomas J, Paulson EK. MR liver imaging and cholangiography in the presence of surgical metallic clips at 1.5 and 3 Tesla. Eur Radiol 2006;16(10):2309-16.

[21] Port JD, Pomper MG. Quantification and minimization of magnetic susceptibility artifacts on GRE images. J Comput Assist Tomogr 2000;24(6):958-64.

[22] Wieben O, Francois C, Reeder SB. Cardiac MRI of ischemic heart disease at 3 Tesla: potentials and challenges. Eur J Radiol 2008; [*same issue as this manuscript*].

[23] Deshpande VS, Shea SM, Li D. Artifact reduction in true-FISP imaging of the coronary arteries by adjusting imaging frequency. Magn Reson Med 2003;49(5):803-9.

[24] Schär M, Kozerke S, Fischer SE, Boesiger P. Cardiac SSFP imaging at 3 Tesla. Magn Reson Med 2004;51(4):799-806.

[25] Michaely HJ, Nael K, Schoenberg SO, Laub G, Reiser MF, Finn JP, Ruehm SG. Analysis of cardiac function--comparison between 1.5 Tesla and 3.0 Tesla cardiac cine magnetic resonance imaging: preliminary experience. Invest Radiol 2006;41(2):133-40.

[26] Zelaya FO, Roffmann WU, Crozier S, Teed S, Gross D, Doddrell DM. Direct visualisation of B1 inhomogeneity by flip angle dependency. Magn Reson Imaging 1997;15(4):497-504.

[27] Kingsley PB, Ogg RJ, Reddick WE, Steen RG. Correction of errors caused by imperfect inversion pulses in MR imaging measurement of T1 relaxation times. Magn Reson Imaging 1998;16(9):1049-55.

[28] Jin JM, Chen J, Chew WC, Gan H, Magin RL, Dimbylow PJ. Computation of electromagnetic fields for high-frequency magnetic resonance imaging applications. Phys Med Biol 1996;41(12):2719-38.

[29] Collins CM, Liu W, Schreiber W, Yang QX, Smith MB. Central brightening due to constructive interference with, without, and despite dielectric resonance. J Magn Reson Imaging 2005;21(2):192-6.

[30] Wald LL, Adalsteinsson E. Parallel-excitation techniques for ultra-high-field MRI. In: Schoenberg SO, Dietrich O, Reiser MF, editors. Parallel imaging in clinical MR applications. Berlin: Springer, 2007:511-21.

[31] Katscher U, Bornert P, Leussler C, van den Brink JS. Transmit SENSE. Magn Reson Med 2003;49(1):144-50.

[32] Zhu Y. Parallel excitation with an array of transmit coils. Magn Reson Med. 2004;51(4):775-84.

[33] Collins CM, Liu W, Swift BJ, Smith MB. Combination of optimized transmit arrays and some receive array reconstruction methods can yield homogeneous images at very high frequencies. Magn Reson Med 2005;54(6):1327-32.

[34] Lufkin R, Anselmo M, Crues J, Smoker W, Hanafee W. Magnetic field strength dependence of chemical shift artifacts. Comput Med Imaging Graph 1988;12(2):89-96.

[35] Smith AS, Weinstein MA, Hurst GC, DeRemer DR, Cole RA, Duchesneau PM. Intracranial chemical-shift artifacts on MR images of the brain: observations and relation to sampling bandwidth. AJR Am J Roentgenol 1990;154(6):1275-83.

[36] Xu Y, Wang Z, Makedon FS, Pearlman JD. BP-neural network based-characterization of electrographic magnetohydrodynamic signals in MR. Conf Proc IEEE Eng Med Biol Soc 2004;1:431-3.

[37] Fischer SE, Wickline SA, Lorenz CH. Novel real-time R-wave detection algorithm based on the vectorcardiogram for accurate gated magnetic resonance acquisitions. Magn Reson Med 1999;42(2):361-70.

[38] Koktzoglou I, Simonetti O, Li D. Coronary artery wall imaging: initial experience at 3 Tesla. J Magn Reson Imaging 2005;21(2):128-32.

[39] Amartur S, Haacke EM. Modified iterative model based on data extrapolation method to reduce Gibbs ringing. J Magn Reson Imaging 1991;1(3):307-17.